Molecular Crystals and Liquid Crystals

ISSN: 1542-1406 (Print) 1563-5287 (Online) Journal homepage: http://www.tandfonline.com/loi/gmcl20

What Are ThresholdLess AntiFerroelectric (TLAF) LCs?–Disordered SmC*-Like Phase with q_T = 1/2 in a Wide Temperature Range

Atsuo Fukuda

To cite this article: Atsuo Fukuda (2015) What Are ThresholdLess AntiFerroelectric (TLAF) LCs?–Disordered SmC*-Like Phase with q_T = 1/2 in a Wide Temperature Range, Molecular Crystals and Liquid Crystals, 610:1, 1-22, DOI: 10.1080/15421406.2015.1025198

To link to this article: http://dx.doi.org/10.1080/15421406.2015.1025198

Published online: 06 Jul 2015.

Mol. Cryst. Liq. Cryst., Vol. 610: pp. 1–22, 2015

ISSN: 1542-1406 print/1563-5287 online
DOI: 10.1080/15421406.2015.1025198

What are ThresholdLess AntiFerroelectric (TLAF) LCs?—Disordered SmC^*-Like Phase with $q_T = 1/2$ in a Wide Temperature Range

ATSUO FUKUDA*

Department of Electronic and Electrical Engineering, Trinity College, University of Dublin, Dublin, Ireland

In the MC881-MC452 binary mixture system developed by MGC, the near-IR Bragg reflection peak is observed in a wide temperature range from 80°C down to room temperature or lower for a narrow concentration region between 54.99 and 57.50 wt.%; the phase responsible for this near-IR Bragg reflection peak can be identified as disordered SmC-like phase with $q_T = 1/2$ – hereafter designated as $SmC^*_D(1/2)$ – which has the TLAF property in the bulk. Four intriguing mechanisms are operative: (1) The critical concentration exists, above which the free energy of SmC^*_A never becomes lower than that of SmC*; (2) The disclination-assisted thermal linkages assure the thermal equilibrium between ferroelectric and antiferroelectric orderings; (3) The long-range interlayer interactions in the quasi-molecular model stabilize the q_T=1/2 state in a wide temperature range; and (4) A ferroelectric hexatic phase exists on the low temperature side of SmC^*_A and the frustration between them stabilizes another q_T=1/2 state which may coalesce into the ordinary one in the intermediate concentration region. In this way coalesced $SmC^*_D(1/2)$ emerges stably. Because of the disclination-assisted thermal linkages, $SmC^*_D(1/2)$ must be disordered and soft with respect to the tilting directions and senses of the in-layer directors even in the bulk; electric-field-induced switching is expected to occur layer by layer but not cooperatively and hence shows the TLAF property.*

PACS numbers: 61.30.Eb; 64.70.M-; 77.80.-e

1. Introduction

About 20 years ago, the Inui mixture and the Mitsui mixture were reported to show the thresholdless, hysteresis-free, V-shaped switching and got publicity for the application to gray-scale liquid crystal displays (LCDs). The structural formulas and the mixing ratios are given in Fig. 1. I anticipated that a ThresholdLess AntiFerroelectric (TLAF) SmC^*-like phase must exist in the bulk [1–3][endnote 68]. Meanwhile, Rudquist *et al.* and Park *et al.* studied the Inui mixture and concluded that it must be ferroelectric; the charge stabilization and the highly collective azimuthal angle rotation of the director on the SmC^* tilt cone in a macroscopic scale are essential in the V-shaped switching [4–7]. Seomun studied the

*Address correspondence to Atsuo Fukuda, currently visiting professor in the Department of Electronic and Electrical Engineering, Trinity College, University of Dublin, Dublin 2, Ireland. E-mail: fukudaa@tcd.ie

Color versions of one or more of the figures in the article can be found online at www.tandfonline.com/gmcl.

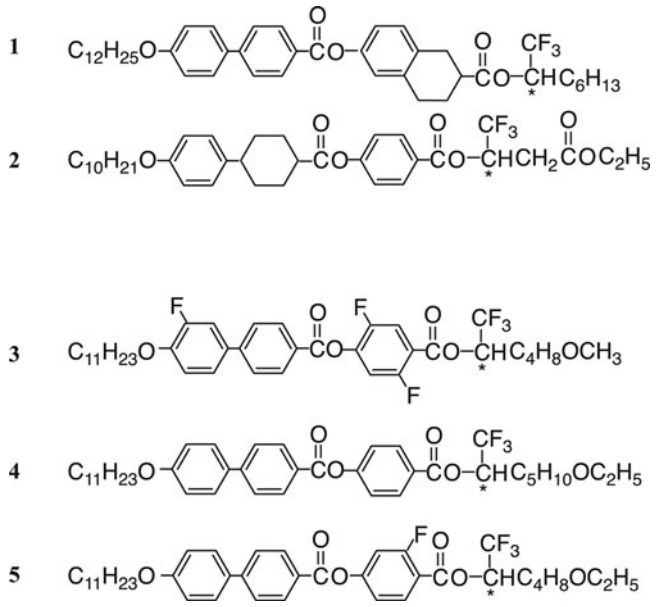

Figure 1. Chemical structural formulas of constituent compounds of the Mitsui mixture (**1**:**2** = 63:37) and the Inui mixture (**3**:**4**:**5** = 40:40:20).

Inui mixture by observing the Bragg reflection spectra due to the helical structure as well as the conoscopic figures under applied electric fields and identified the phase sequence as SmC_A^*–a ferrielectric phase–Sm*A* [8, 9]. Since the Inui mixture is the ternary mixture system and the sample amount available at that time was very limited, it has not been thoroughly investigated. In view of the fact that the melatopes may appear not only perpendicular but also parallel to an applied electric field in ferroelectric LCs as clarified by Song *et al.* [10], the phase identified as ferrielectric by Seomun must be considered to be ferroelectric. At the same time, however, it is questionable whether q_T is really 1; it is possible that $q_T \gtrsim 0.99$ but not 1 as was actually found in the MC881-MC452 binary mixture system [11, 12].

Since the Mitsui mixture is the binary mixture system, on the other hand, Seomun *et al.* [13] obtained the temperature-mixing ratio ($T - r$) phase diagram of compounds **1** and **2** using (a) thick free-standing films and (b) thin homogeneous cells as reproduced in Fig. 2. The sample amount was also restricted, and Seomun *et al.* was not successful in pinpointing the emergence of TLAF in the bulk (thick free-standing films) [endnote 69]. In thin homogeneous cells, however, Seomun *et al.* confirmed that the V-shaped switching in thin cells occurs even in the region where the antiferroelectric phase exists in the bulk, and that this is not due to the electric-field-induced ferroelectric state [14, 15]. Moreover, Hayashi *et al.* firmly established, by observing the Raman scattered light at the tip of the V under dynamically applied electric fields, that the V-shaped switching of the apparently antiferroelectric phase in the bulk is not due to the highly collective azimuthal angle rotation of the director on the SmC^* tilt cone in a macroscopic scale [16, 17]; the obtained distribution of the local in-plane directors at the tip of the V is considerably broad in the Mitsui mixtures, whereas it is narrow in the first component of the Inui mixture. In the Mitsui mixture with **1**:**2** = 63:37, no antiferroelectric phase stably exists in thin cells because the threshold does not emerge even in the first run although it does in the bulk.

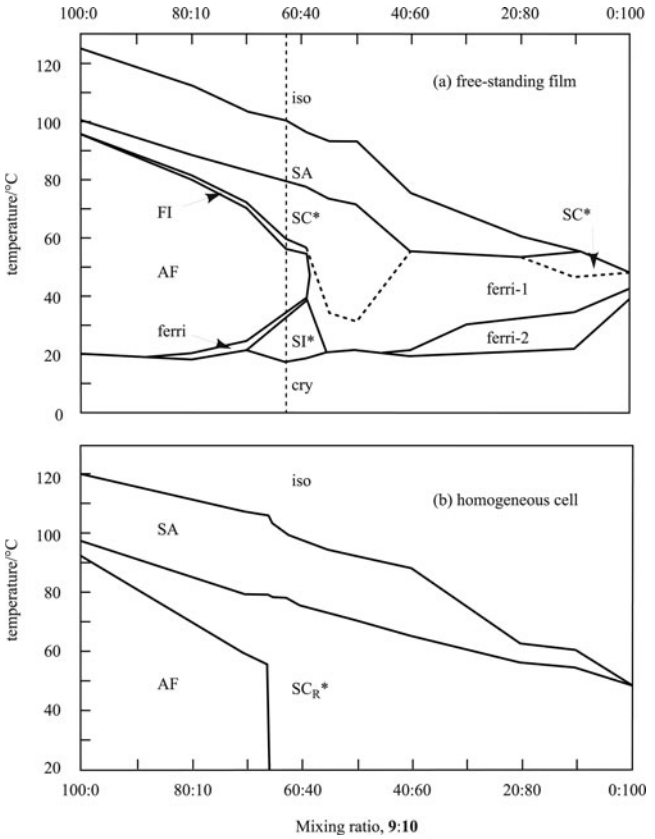

Figure 2. Temperature-mixing ratio ($T - r$) phase diagram of compounds **1** and **2** obtained (a) using a thick free standing film and (b) using a thin homogeneous cell. At least the phase identified as ferri-1 by conoscopy must be SmC^*, because the melatopes may appear not only perpendicular but also parallel to the applied electric field in ferroelectric LCs [10]; in fact, the boundaries between SmC^* and ferri-1 are drawn by dotted lines. (From Ref. [13])

Two Japanese companies, Casio and Toshiba, prototyped their TLAF-LCDs, using nominally TLAF materials produced by two Japanese chemical companies, MGC [18] and Mitsui Chemicals, respectively. In the publications on TLAF-LCDs driven by active matrix, the chemical structures of their TLAF materials were not disclosed [19–24]. Moreover, it was hard to obtain plenty of the most likely candidate TLAF materials from any chemical companies during active periods of developing their materials. What we were able to do was to just insist on an important role of the frustration between ferroelectricity and antiferroelectricity by studying thin cell properties using a small amount of TLAF materials, even peripheral and not most-likely, such as the Inui and Mitsui mixtures. We could not pinpoint the frustration phenomena in the bulk clearly.

Ironically, a breakthrough has come through their failure in the commercialization of TLAF materials. When MGC stopped the R & D of TLAF materials in 2006, they kindly donated large amounts of key compounds to me, the chemical structural formulas of which are shown in Fig. 3 [18]. The most important compounds appear to be MC881 and MC815. Their basic idea is to prepare binary mixtures of two strong antiferroelectric

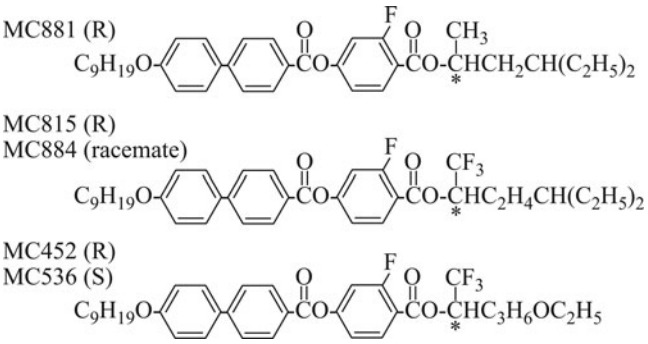

Figure 3. Chemical structural formulas of key compounds developed by MGC. MC881is antiferroelectric, whereas MC815,MC452, and MC536 are ferroelectric, in a wide temperature range [10, 18].

and ferroelectric compounds and to obtain the TLAF state near the boundary [endnote 70]. The binary mixture phase diagram, though rather primitive, is given in Fig. 1 of their Euro. Pat. Appl. [18]. The racemate compound of MC815, i.e. MC884, is used to reduce the spontaneous polarization of TLAF. Although MC452 is a previous generation compound, I'll take up the MC881-MC452 binary mixture system here, since Sandhya *et al.* have clarified the intriguing aspects of frustration in the bulk [11, 12]. The MC881-MC452 binary mixture system they studied shows a very favorable feature; the Bragg reflection due to the macroscopic helical structure of the in-layer directors is observed in the near-UV, visible, or near-IR wavelength region in the almost entire temperature range covering SmC_A^* and SmC^*.

Notice, however, that some similar, though preliminary, results have also been obtained in the MC881-MC815 and MC881-MC884 binary mixture systems [26, 27]. In this paper I will clarify what is the ThresholdLess AntiFerroelectric (TLAF) phase in the bulk of the MC881-MC452 binary mixture system.

2. Reviews of the $T - r$ Phase Diagram Obtained by Sandhya *et al.*

Let us begin with reviewing the peculiar aspects of the phase diagram in the bulk of the MC881-MC452 binary mixture system shown in Fig. 4; the ordinate is temperature and the abscissa is MC452 concentration [11, 12]. Putting aside minor details, we can say the left-side blue area is antiferroelectric and the right-side red area is ferroelectric. When we try to determine the boundary precisely, however, we notice that it's impossible. The impossible is most clearly experienced when we observe the Bragg reflection spectra due to the macroscopic helical structure of the directors. We plotted Bragg reflection peaks as a function of temperature for various MC452-concentration mixtures, and obtained such three characteristic patterns as reproduced in Fig. 5: Low concentration pattern, High concentration pattern, and in-between, Intermediate pattern in a concentration region as narrow as about 3 wt.%. Peculiar things happen in each region.

First let's take a detailed look at the low-concentration pattern. In pure MC881, the half-pitch band is observed in the short wavelength region on the edge of the intrinsic absorption. The phase transition occurs directly from SmC_A^* to SmA at a temperature above 100°C; ferroelectric SmC^* does not emerge. As the MC452 concentration increases, SmC_A^* moves

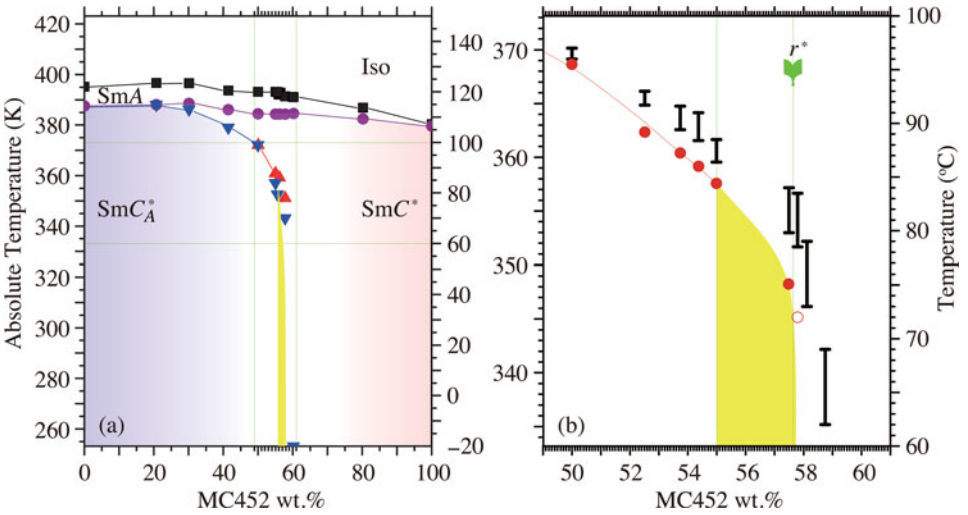

Figure 4. Bulk phase diagrams of MC881-MC452 binary mixture system. (a) Global temperature–concentration ($T - r$) phase diagram, where the apparent phase boundaries were determined by monitoring the dielectric response, spectroscopic Bragg reflection, and electric-field-induced birefringence [25]. (b) Expanded one near the critical concentration $r^* = 57.65 \pm 0.15$ wt.%, where it was found basically impossible to specify the phase transition temperature between SmC_A^* and SmC^*. Bars indicate the temperature ranges where the full-pitch band emerges and shows a rapid growth as the temperature rises. When the divergence or its indication can be seen in the half-pitch band, the divergence temperatures are also given as red circles: closed ones in the case of a steep half-pitch rise on both the low- and high-temperature sides, while open ones in the case of a clear rise on the high-temperature side only [12]. As concluded in this paper, the TLAF SmC_D^*(1/2) phase emerges in the yellow area.

toward the shorter wavelength side and becomes buried under the intrinsic absorption, whereas apparently ferroelectric SmC^* begins to emerge. At 50 wt.%, for example, both full-pitch and half-pitch bands almost suddenly emerge at the same time, apparently when the phase transition occurs from antiferroelectric SmC_A^* to ferroelectric SmC^*. As the concentration increases further, a peculiar transitional region comes to be conspicuous. Even at 50 wt.%, we can see the transitional region, though very narrow. The transitional region becomes remarkably wider in temperature as the concentration slightly increases further. For example, at 53.74 wt.%, the half-pitch reflection peak wavelength gradually increases, diverges, and then comes back to the visible region. The circular polarization changes its handedness from right to left at the divergence. The full-pitch reflection band emerges on the high temperature side of the divergence. As you see, antiferroelectric SmC_A^* appears to change into ferroelectric SmC^* continuously.

The bulge and the IR reflection branch at 53.74 wt.% in the low concentration region come to play a major role in the intermediate region. In fact, at 54.99 wt.%, the IR half-pitch reflection pattern emerges stably over a wide temperature range from less than 30 to above 80°C. By overlapping two low concentration plots, 54.37 and 53.74 wt.%, we can see how the bulge and the IR reflection branch coalesce into the IR half-pitch reflection pattern in the intermediate concentration region. The evolution occurs rather continuously from the low to the intermediate. On the other hand, the intermediate pattern changes into the high concentration pattern abruptly as seen by comparing 57.50 and 57.79 wt.%. The difference

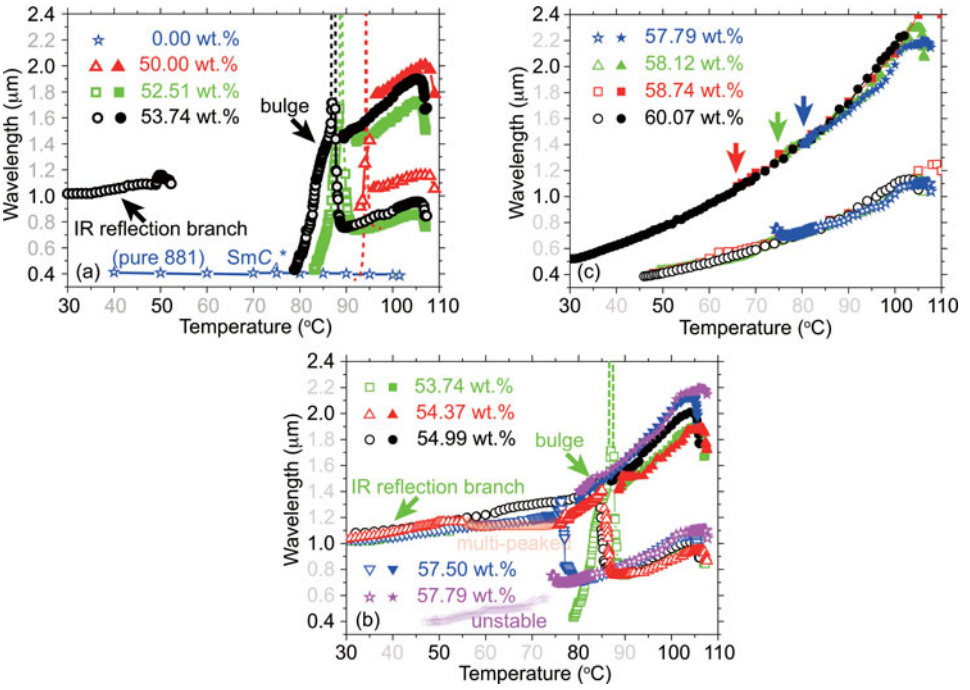

Figure 5. Temperature dependence of the Bragg reflection peak at various MC452 concentrations near the critical concentration r^*. (From Ref. [12])

is less than 0.3 wt.%, but at 57.79 wt.%, both half-pitch and full-pitch reflection bands are hardly observed in the low temperature region. This may mean that 57.79 wt.% is very close to the critical concentration r^*.

At 58.12 wt.%, the half-pitch band emerges in the whole observable temperature range, but the full-pitch band does not emerge at lower temperatures and appears at a particular temperature as indicated by an arrow. As the MC452 concentration increases further, the full-pitch-band emergence occurs at lower temperatures as indicated by arrows. Peculiarly,

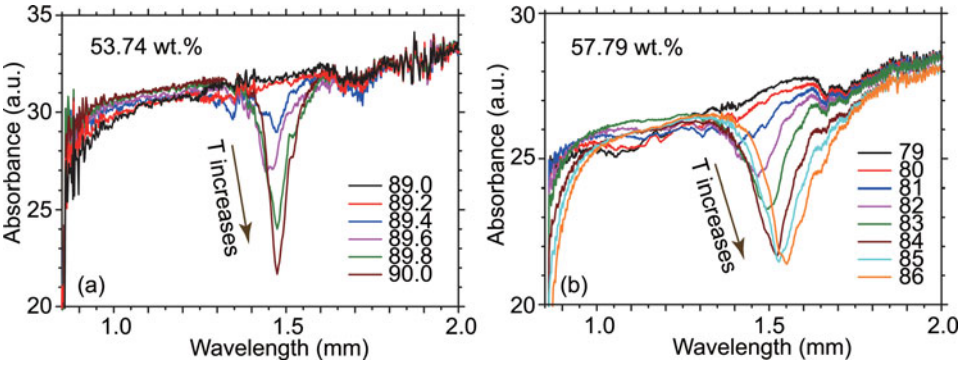

Figure 6. The gradual growth of the full-pitch band. The growing temperature range becomes wider near the critical concentration r^*. (From Ref. [12])

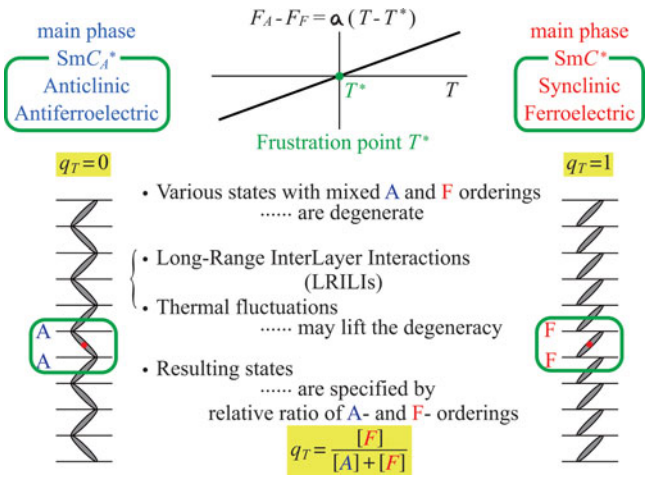

Figure 7. Illustration of frustration between SmC_A^* and SmC^* together with degeneracy lifting at the frustration point.

the emergence of the full-pitch band does not change the handedness of the half-pitch band. Even more peculiarly, the full-pitch band emerges gradually over a wide temperature range, say more than 5°C as illustrated in Fig. 6. In the low concentration region, the full-pitch band emergence occurs also gradually although the temperature range is narrow.

In this way, some gradual continuous changes are taking place in all the concentration regions from antiferroelectric SmC_A^*-like states to ferroelectric SmC^*-like states. I would like to insist that the IR half-pitch reflection pattern in the intermediate concentration region is a manifestation of the TLAF phase in the bulk. Let me explain how we can reach this conclusion.

3. Frustration between SmC_A^* and SmC^*

Briefly speaking, we are dealing with the frustration between SmC_A^* and SmC^* as illustrated in Fig. 7 [28, 29]. The tilting ordering between adjacent layers is anticlinic antiferroelectric in SmC_A^*, whereas it is synclinic ferroelectric in SmC^*. Hereafter we use abbreviations, A-ordering and F-ordering, respectively. At the phase transition temperature T^*, that is the frustration point, various states with mixed A- and F-orderings are degenerate. Long-Range InterLayer Interactions (LRILIs) or thermal fluctuations may lift the degeneracy. And the resulting states are specified by the relative ratio of A- and F-orderings,

$$q_T = \frac{[F]}{[A]+[F]}. \tag{1}$$

So SmC_A^* has $q_T = 0$, whereas SmC^* has $q_T = 1$. Let us try to understand the realization of the TLAF state on the basis of the degeneracy lifting due to thermal fluctuations and LRILIs. We follow four steps.

3.1. Short-Range InterLayer Interactions (SRILIs)

The first step is the Short-Range InterLayer Interactions (SRILIs) and the characteristic phase diagram shown in Fig. 4. The sudden change from 57.50 to 57.79 wt.% experimentally

observed in Fig. 5(b) appears to indicate the existence of a critical concentration r^*, above which SmC_A^* becomes absolutely unstable. So let us consider to what extent the r^* existence can be explained by the molecular model for anticlinic antiferroelectric SmC_A^* [30–33], where the orientational correlations between transverse molecular dipoles stabilize SmC_A^* with respect to synclinic ferroelectric SmC^*. The free energy difference between SmC_A^* and SmC^*, normalized by $k_B T_c$, is written in its dimensionless form as

$$\tilde{F}_A - \tilde{F}_F = \sin^2 2\theta \left(-\frac{\tilde{d}_\perp^4}{\tilde{T}\cos^6\theta} - \tilde{V}_{||} \right). \tag{2}$$

Here $\tilde{T} = T/T_c$, T_c is the temperature of the phase transition to SmA, and $\tilde{d_\perp}$ is the dimensionless transverse dipole moment. The first term represents the orientational correlations between transverse molecular dipoles in adjacent layers and tends to stabilize SmC_A^*. The second term $\tilde{V}_{||} < 0$ represents a contribution from all other relevant interactions between adjacent layers stabilizing SmC^*. Since the tilt angle generally decreases monotonically with temperature, SmC^* is always a higher temperature phase than SmC_A^* when both emerge.

Suppose the tilt angle θ is given as a function of the normalized temperature $\tilde{T}$, we can draw a simple phase diagram, $\tilde{d_\perp}^4/|\tilde{V}_{||}|-\tilde{T}$, that contains Sm$A$, Sm$C^*$, and Sm$C_A^*$. The ordinate $\tilde{d_\perp}^4/|\tilde{V}_{||}|$ stands for the relative strength ratio of antiferroelectricity and ferroelectricity, which must monotonically decrease as the MC452 concentration r increases. In the molecular model, the tilt angle θ is considered to be mainly determined by the term,

$$\tilde{F}_\perp(\theta) = \frac{1}{2}\alpha(\tilde{T} - 1)\sin^2\theta + \frac{1}{4}B\sin^4\theta\,, \tag{3}$$

that stems from intermolecular interactions within one smectic layer and is equivalent to the familiar Landau-de Gennes expansion in powers of the tilt angle θ. Thus we obtain the temperature dependence,

$$\theta = \sin^{-1}\sqrt{\alpha/B(1-\tilde{T})}, \tag{4}$$

which gives the boundary between SmC_A^* and SmC^* as shown by solid lines in Fig. 8. Equation (4) may well describe the temperature dependence of the tilt angle θ near the second-order phase transition to SmA. Since θ does not show any saturation and keeps increasing up to 90°, however, Eq. (4) could not be used in the lower temperatures separated from T_c.

It is not easy to obtain the tilt angle temperature dependence $\theta(\tilde{T})$ theoretically on the basis of any molecular models. Emelyanenko and Ishikawa [34] tried to improve Eq. (4) phenomenologically; they qualitatively explained the boundary between SmC_A^* and SmC^* in Fig. 4 by assuming that the relative strength ratio of antiferroelectricity and ferroelectricity $\tilde{d_\perp}^4/|\tilde{V}_{||}|$ must monotonically decrease as the MC452 concentration r increases. Experimentally, the temperature dependence of tilt angle θ and spontaneous polarization P_s were measured in MC881 and MC815 as shown in Fig. 2 of Ref. [35] and Fig. 8 of Ref. [10]. At the phase transition from SmA to SmC_A^* or SmC^*, a tilt angle as large as 25° or more suddenly emerges and the corresponding large spontaneous polarization is produced abruptly. The temperature variation of spontaneous polarization in MC452 given in Fig. 14 of Ref. [25] indicates the similar behavior; a considerably large tilt angle abruptly appears at the first-order phase transition and rather promptly saturate at lower temperatures. By assuming $\theta = const.$, we obtain the boundary between SmC_A^* and SmC^*

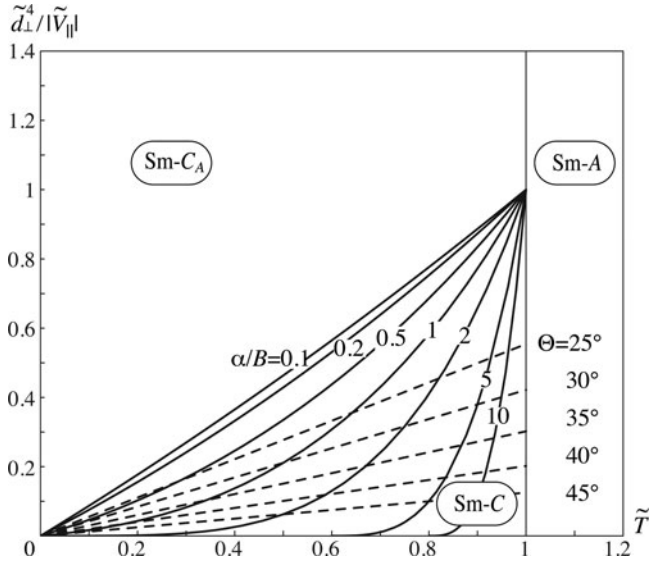

Figure 8. $\tilde{d_\perp}^4/|\tilde{V}_{||}|-\tilde{T}$ phase diagram. The boundary between SmC_A^* and SmC^* depends on the tilt angle $\theta(\tilde{T})$; solid and dotted lines are obtained by using Eq. (4) and by assuming $\theta = const.$, respectively.

as shown by dotted lines in Fig. 8. Because of the $1/\tilde{T}$ temperature dependence of the first term in Eq. (2), SmC_A^* is always stabilized at lower temperatures and never becomes absolutely unstable even when the tilt angle is constant at lower temperatures; hence the aforementioned molecular model [30–33] alone cannot explain the presence of the critical concentration r^*, i.e. the abrupt change from 57.50 to 57.79 wt.% experimentally observed in Fig. 5(b). We need some other SRILIs discussed later in Sec. 3.4.

3.2. Degeneracy Lifting due to Thermal Fluctuations — Disclination-Assisted Thermal Linkage between SmC_A^* and SmC^* —

Some continuous changes from antiferroelectric SmC_A^*-like states to ferroelectric SmC^*-like states reviewed in Sec. 2 prompt us to say farewell to the absolute zero temperature approximation. We now head for the second step: the thermal linkage between SmC_A^* and SmC^* minima [11, 12]. Usually we do not consider this linkage, because thermal transition between two macroscopic states can hardly occur, when they are separated by a finite potential barrier. In other words, the well-established tilted smectic structure suppresses the thermal excitation of cooperative director motion of the antiphase mode which promotes the transition between SmC_A^* and SmC^*. The actual phase transition occurs, however, through solitary wave propagation in a non-uniform disclination-assisted way but not through the antiphase mode in a uniform way [36–39]. So we can now consider such a system consisting of N smectic layer boundaries, each of which takes either of A-ordering or F-ordering, as illustrated in Fig. 9. Because of the disclination-assisted thermal linkage between the orderings, their ratio is given by the Boltzmann distribution [11, 12],

$$\frac{[A]}{[F]} = \exp\left(-\frac{\Delta E}{k_B T}\right), \tag{5}$$

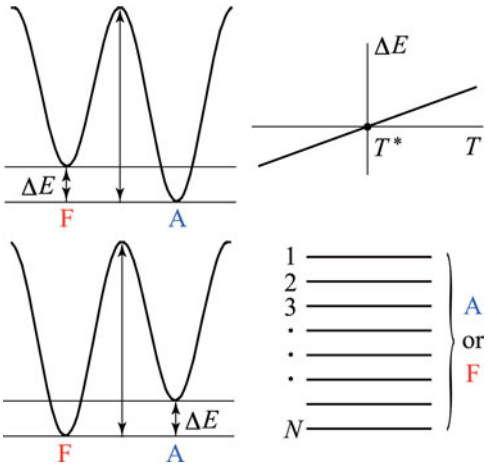

Figure 9. Illustration of disclination-assisted thermal linkage between SmC_A^* and SmC^*.

where ΔE is usually considered to change linearly with temperature near the frustration temperature

$$\Delta E = E_A - E_F = \alpha^*(T - T^*)\,. \tag{6}$$

Thus we obtain the temperature dependence of q_T defined by Eq. (1),

$$q_T = \frac{1}{1 + \exp\{-(\alpha^*/k_{\mathrm{B}})(T - T^*)/T\}}\,. \tag{7}$$

Since the macroscopic helical-ptich $p(q_T)$ is empirically given by [40–42]

$$\frac{1}{p(q_T)} = \frac{q_T}{p(1)} + \frac{1 - q_T}{p(0)}\,, \tag{8}$$

we also obtain the temperature dependence of $p(q_T)$ by inserting Eq. (7) into Eq. (8). Here $p(1)$ and $p(0)$ are the macroscopic helical long-pitches of SmC^* and SmC_A^*, which have the opposite signs depending on the handedness of the helices [40–42] and are experimentally estimated. In this way, by considering α^*/k_{B} and T^* as phenomenological adjustable parameters, we can reproduce the observed peak vs. temperature data in the high temperature region, as shown in Fig. 10; the parameters used together with $p(0)$ and $p(1)$ are given in the figure. At the same time, we can draw q_T as a function of temperature like the red curve. By expanding the ordinate scale 100 times, we obtain the blue curve.

We now notice that the full-pitch band begins to grow at around $q_T = 0.991$. In other words, the full-pitch band disappears by mixing 1 wt.% anticlinic antiferroelectric ordering in ideal SmC^*. Similar results are obtained both in the low and intermediate concentration regions and hence considered pretty general. So we tried to simulate the growing process by appropriately introducing disclination defects, and successfully reproduced the gradual growth of the full-pitch band occurring between $q_T = 0.991$ and 0.999. A solitary wave propagation causes a simultaneous change in the tilting sense of some neighboring layers and produces a pair of π-discrination defects. Since the defect pairs must be distributed

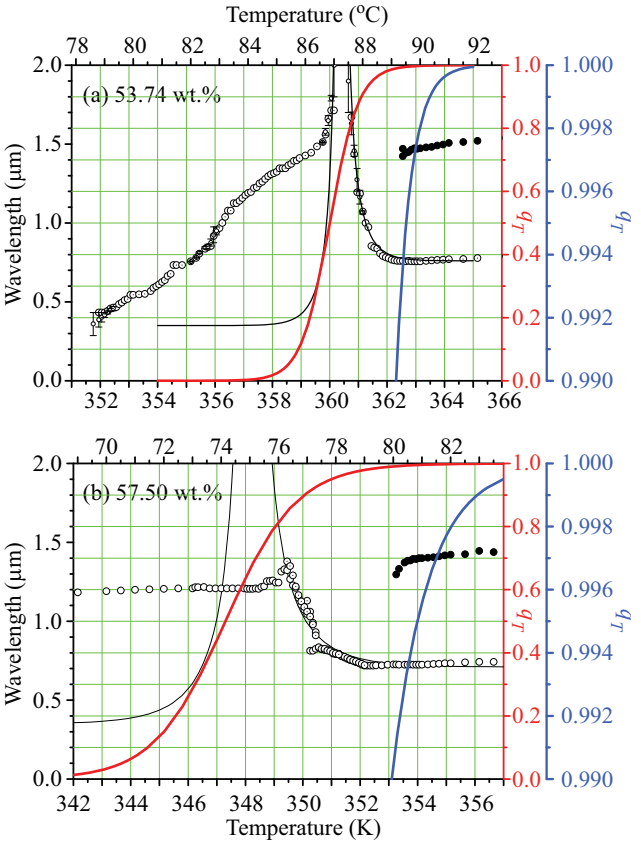

Figure 10. Observed Bragg reflection peak vs temperature in (a) 53.74 wt% and (b) 57.50 wt%, which is fitted by Eq. (8) using Eq. (7) using indicated parameter values. Also given by red and blue curves is q_T as a function of temperature. Conspicuous growing of the full-pitch band is observed in the yellowed temperature and q_T ranges. (From Ref. [12])

randomly throughout the bulk and their average number is

$$\frac{1}{2}(1 - q_T)\,, \tag{9}$$

where q_T is given as function of T in Eq. (7). The only additional parameters necessary to simulate the superlattice structure at T is the defect separation of a pair

$$n = \lfloor\!\lfloor\, x + 0.5 \,\rfloor\!\rfloor \tag{10}$$

in the unit of the number of smectic layers, where x is assumed to be given by random numbers distributed normally with mean μ and standerd deviation σ smectic layers

$$\frac{1}{\sqrt{2\pi}\sigma} \exp\left\{-\frac{(x-\mu)^2}{2\sigma^2}\right\}. \tag{11}$$

We have calculated the Bragg reflection spectra by using Berreman's 4×4 matrix method for randomly produced superlattice structures and averaged them.

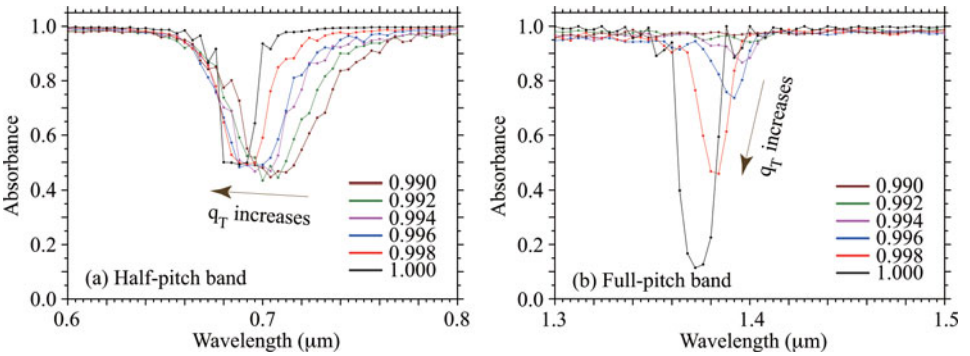

Figure 11. Simulated Bragg reflection spectra in a homogeneous cell with 15000 smectic layers with 3.5 nm thickness for a light beam incident at 20° by changing the wavelength from 0.35 to 2.5 μm at 4-nm intervals. Parameters used are $\mu = 200$ and $\sigma = 50$; values given in the figure are those of q_T. (From Ref. [12])

Figure 11 illustrates the results which successfully reproduce the growth of the full-pitch band at around $q_T \approx 0.991 \sim 0.999$. Thus we can understand the observed gradual growth of the full-pitch band in the temperature range depending on the concentration, less than 1°C in the low concentration and as wide as 5°C in the intermediate concentration. In this way, the disclination-assisted thermal linkage between A and F orderings can explain the Bragg reflection spectra quite well in the higher temperature region. But in the lower temperature region, it does not work at all. This is because the degeneracy lifting is also caused by LRILIs [43–51]. So let's review the LRILIs as the third step.

3.3. Degeneracy Lifting due to Long-Range InterLayer Interactions (LRILIs)

The LRILIs proposed by Emelyanenko and Osipov [43] are simple and effective in understanding the degeneracy lifting at the frustration point in the MC881-MC452 binary mixture system, where the tilt angle can be approximately considered constant as is already pointed out in Sec. 3.1. They numerically calculated the subphase superlattice structures and the stability ranges by using the free energy,

$$F = \sum_{i=1}^{N} (F_i + \Delta F_i), \tag{12}$$

where N is the total number of smectic layers. The polarization-independent part F_i is phenomenologically given by

$$F_i = -\frac{a\,(T - T^*)}{T^*}(\cos\phi_{i-1,i} + \cos\phi_{i,i+1})$$

$$-b\,(\cos^2\phi_{i-1,i} + \cos^2\phi_{i,i+1}), \tag{13}$$

where $a >$ and $b > 0$ are constants, and T^* is the transition temperature between synclinic ferroelectric SmC^* and anticlinic antiferroelectric SmC^*_A, which are stabilized for $T > T^*$ and $T < T^*$, respectively.

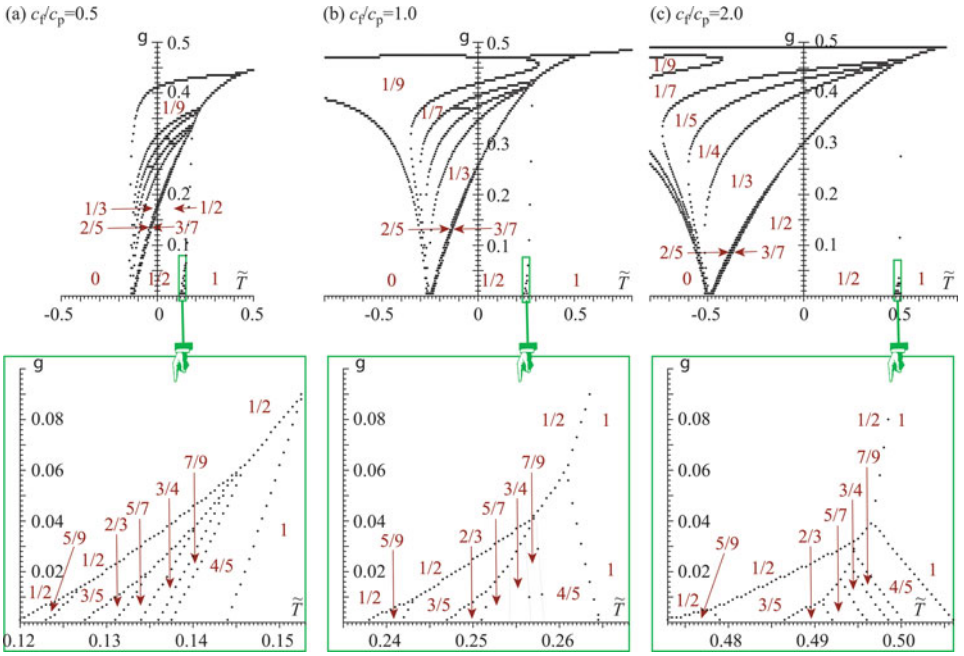

Figure 12. Recalculated g–$\tilde{T}$ phase diagrams with $\chi c_p c_f/\tilde{b} = 0.12$ by taking account of superlattice structures consisting of up to 10 smectic layers, (a) c_f/c_p=0.5, (b) c_f/c_p=1.0, and (c) $c_f/c_p = 2.0$. All the subphases appear in the increasing order of q_T. Notice that $q_T = 2/5$ and 3/7 emerge between 1/3 and 1/2 and that several subphases with $q_T > 1/2$ also emerge in a very squeezed area which is expanded in the lower part. See text for details.

The polarization-dependent part ΔF_i is written as

$$\Delta F_i = \frac{1}{2\chi}\{\mathbf{P}_i^2 + g\,(\mathbf{P}_{i-1}\cdot\mathbf{P}_i + \mathbf{P}_i\cdot\mathbf{P}_{i+1})\} + c_p(\mathbf{P}_i\cdot\boldsymbol{\xi}_i) + c_f\cos\theta\,(\mathbf{P}_i\cdot\Delta\mathbf{n}_{i\pm1}), \tag{14}$$

which consists of the last two terms containing the piezoelectric and flexoelectric coefficients, c_p and c_f, as well as the first term of the polarization-polarization interactions. Here g represents the molecular positional correlation in adjacent layers and $\boldsymbol{\xi}_i \equiv \cos\theta\,[\mathbf{n}_i \times \mathbf{e}]$. The tilt angle θ is assumed to be temperature-independent and spatially uniform. They reasonably took account of the direct couplings between adjacent layers only; it is hard to consider any direct coupling between smectic layers separated in next-nearest-neighbor positions or beyond, since smectic LCs have no long-range positional order.

When minimizing the total free energy F in Eq. (12) with respect to polarization $\mathbf{P}_i$, however, we obtain effective LRILIs. By reference to f_k, $f_k^{(1)}$, and $f_k^{(2)}$ given in Eqs. (61) and (63) of Ref. [43], the modified free energy per single layer of a biaxial subphase with a t-layer unit cell is represented by

$$\tilde{F} = -\frac{\tilde{a}\,(T - T^*)/(\tilde{b}\,T^*)}{t}\sum_{i=0}^{t-1}\cos\varphi_{i,i+1} - \frac{1}{t}\sum_{i=0}^{t-1}\cos^2\varphi_{i,i+1}$$

$$-\frac{\chi c_{\rm p}c_{\rm f}/\tilde{b}}{2}\{(c_{\rm p}/c_{\rm f})f_0+(c_{\rm f}/c_{\rm p})f_0^{(2)}\}$$
$$-\frac{\chi c_{\rm p}c_{\rm f}/\tilde{b}}{t}\sum_{i=0}^{t-2}\sum_{j=i+1}^{t-1}\{(c_{\rm p}/c_{\rm f})f_{j-i}+(c_{\rm f}/c_{\rm p})f_{j-i}^{(2)}\}\cos\varphi_{i,j}$$
$$+\frac{2\,\chi c_{\rm p}c_{\rm f}/\tilde{b}}{t}\sum_{i=0}^{t-2}\sum_{j=i+1}^{t-1}f_{j-i}^{(1)}\sin\varphi_{i,j}. \tag{15}$$

Four dimensionless parameters are needed: g represents the molecular positional correlation in adjacent layers and is explicitly contained in f_k, $f_k^{(1)}$, and $f_k^{(2)}$, $\tilde{T}=\tilde{a}\,(T-T^*)/(\tilde{b}\,T^*)$ the modified temperature, $c_{\rm f}/c_{\rm p}$ the ratio between flexoelectric and piezoelectric coefficients, and the final one $\chi c_{\rm p}c_{\rm f}/\tilde{b}$ represents the relative strength of the effective LRILIs.

Biaxial subphases are nonplanar, but the actual structure does not deviate largely from the corresponding planar prototype. Given the clinicity of a t-layer unit cell by assigning 0 or π for $\alpha_i^0\equiv\varphi_{i,i+1}^0$, Eqs. (67)– (69) of Ref. [43] ensure that we can uniquely determine the small deviation angle $\Delta\alpha_i\equiv\Delta\varphi_{i,i+1}$ that minimize the modified free energy of Eq. (12). Since there exists a serious typographical error in Eq. (69) of Ref. [43], we reproduce the corrected Eqs. (67)– (69) in Appendix. After checking all the possible sequences of α_i^0, we obtain the optimal structure of the biaxial subphase with the t-layer unit cell. Finally, the free energies of phases with different-size unit cells are compared with one another to select the phase that corresponds to the global minimum at a given temperature $\tilde{T}$ for a particular choice of the model parameters.

Figure 12 is the $g-\tilde{T}$ phase diagrams thus obtained. Another changeable parameter is $c_{\rm f}/c_{\rm p}$, since the fourth parameter $\chi c_{\rm p}c_{\rm f}/\tilde{b}$ is experimentally estimated to be 0.12 as explained later. The phase diagram with $c_{\rm f}/c_{\rm p}=1.0$ looks the same as the one given in Fig. 6 of Ref. [43]; qualitatively, it does not change much for $c_{\rm f}/c_{\rm p}=0.5$ or 2.0 at least when g is as small as 0.25 or less. We only take account of the short-range interactions between adjacent layers in Eq. (12), but can explain the staircase character of the subphase emergence and its distinctive asymmetric appearance. As you see in the $g-\tilde{T}$ phase diagrams, many subphases with $q_T\leqq 1/2$ have their stable emerging area, but subphases with $q_T>1/2$ do not emerge stably and are squeezed into a narrow area. The staircase looks quite asymmetric with respect to $q_T=1/2$. Moreover, the $q_T=1/2$ subphase itself is very characteristic in comparison with other subphases, as illustrated in Fig. 13. It stably exists even at $g=0$ in a wide temperature range, and the structure is characterized by a single non-planar deviation angle,

$$\delta=\Delta\alpha_2=\Delta\varphi_{2,3}=\chi\,|\,c_{\rm p}c_{\rm f}\,|\,/\tilde{b}, \tag{16}$$

which is uniquely determined by the aforementioned fourth dimensionless parameter. The structure is well characterized experimentally so that $\delta=7^\circ=0.12$ rad [52].

No stable emergence of the $q_T>1/2$ subphases in Fig. 12 is consistent with the fact that Eq. (8) can only reproduce the higher temperature part of the observed peak vs. temperature curves in Fig. 10. Since q_T=1/2 for T=T^* in Eq. (7) and the q_T=1/2 subphase stably exists even for $\tilde{T}>0$ in Fig. 12, i.e. $T>T^*$ in Eq. (7), the reasonable reproduction is to be observed for $q_T>1/2$. Actually, the reproduction is rather good for $q_T\gtrsim 0.5$ in (a) 53.74 wt.% and for $q_T\gtrsim 0.8$ in (b) 57.50 wt.%. In these high temperature regions, the degeneracy lifting at the frustration point is considered to be caused by thermal fluctuations alone. In other words, the disclination-assisted thermal linkage between SmC_A^* and SmC^* assures the Boltzmann

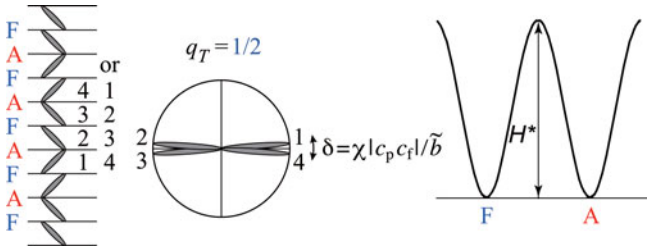

Figure 13. Characteristic $q_T = 1/2$ structure. It stably exists even at $g = 0$ in a wide temperature range and the non-flat angle δ depends on the fourth parameter only, but not on g and c_f/c_p. The sign of $c_p c_f$ determines the handedness of the microscopic short-pitch helical structure. The structure is also well characterized experimentally [52, 53].

distribution between them. In the lower temperature regions, on the other hand, there is a complex interplay between LRILIs and thermal fluctuations.

When the MC452 concentration is low, the effective LRILIs produce a variety of subphases in a temperature region of $0 < q_T \leqq 1/2$. The disinclination-assisted thermal linkages among these subphases make it difficult to distinguish each subphase separately and hence the apparently continuous change is observed in Fig. 10(a). At the same time, the plateaus and the bulge observed in Fig. 10(a) must correspond to some simple subphases with q_T=1/5, 1/4, 1/3, and 1/2, although the detailed identification remains to be studied in the near future [12].

When the MC452 concentration increases and approaches the critical concentration r^*, the IR half-pitch reflection pattern (band) is observed in a wide temperature range from 80 to 30°C or lower probably down to −20°C as shown in Fig. 5(b). It is anticipated to correlate this IR pattern (band) to the q_T=1/2 subphase which becomes exceptionally stable as compared with other subphases when g is approaching zero as seen in Fig. 12. Since the orientational correlations between transverse molecular dipoles in adjacent layers are considered to stabilize SmC_A^* in the molecular model, g must be reasonably larger in SmC_A^* than in SmC^* [30, 33]. The sudden change from 57.50 to 57.79 wt.% shown in Fig. 5(b) seems to indicate that SmC_A^* becomes absolutely unstable above r^*; suppose this is the case, a decrease in g and hence the exceptional stabilization of the q_T=1/2 subphase must occur just below r^*. Actually, however, SmC_A^* is always stabilized below SmC^* in the molecular model explained in Sec. 3.1. Fortunately, another responsible mechanism is suggested by the observed change in the Bragg reflection peak between the low and intermediate concentration regions. Let us consider the details in the next section.

3.4. A Mechanism Stabilizing Another $q_T = 1/2$ Subphase

Lastly, the fourth step is the other mechanism stabilizing the IR half-pitch reflection pattern, which is also related with the presence of the critical concentration r^*, i.e. the abrupt change from 57.50 to 57.79 wt.% experimentally observed in Fig. 5(b). You may remember, at 53.74 wt.%, the emergence of the IR-reflection branch around room temperature and the presence of the bulge just below the divergence. They coalesce into the IR half-pitch reflection pattern with increasing the MC452 concentration as pictured in Fig. 14. To understand the emergence of the IR-reflection branch and its coalescence into the the IR half-pitch reflection pattern, we need the frustration of SmC_A^* not only with SmC^* at higher temperatures but also with HxI^* or re-entrant SmC^* at lower temperatures. The

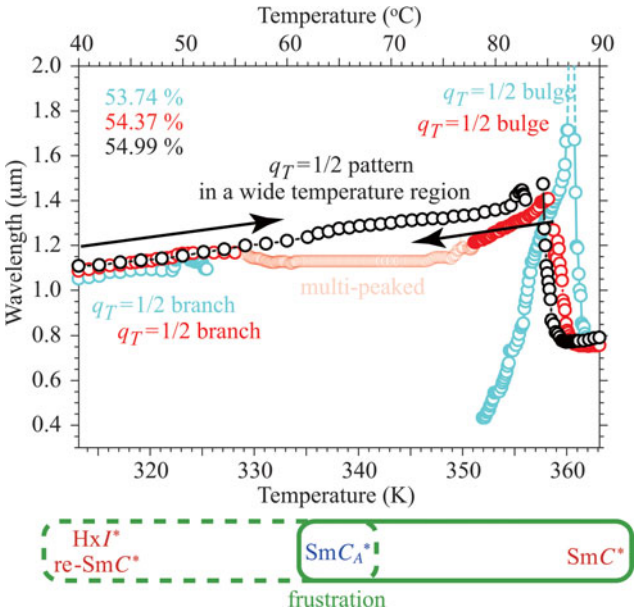

Figure 14. The frustration of SmC_A^* not only with SmC^* at higher temperatures but also with HxI^* or re-entrant SmC^* at lower temperatures. This is needed to understand the emergence of the IR-reflection branch around room temperature together with the bulge just below the divergence at 53.74 wt.% and their coalescence into the IR half-pitch reflection pattern at 54.99 wt.%.

two kinds of frustration produce two similar q_T=1/2 states, which can coalesce into a single one responsible for the IR half-pitch reflection pattern. Such two kinds of frustration and the resulting subphases, although preliminary, were reported by Seomun *et al.* in the Mitsui mixture as reproduced in Fig. 2. The existence of both re-entrant SmC^* and the ferroelectric hexatic phase as well as the first-order transition between them were also reported by Novotna *et al.* [54]; their result as reproduced in Fig. 15 clearly indicates the presence of the critical concentration r^* above which SmC_A^* becomes absolutely unstable.

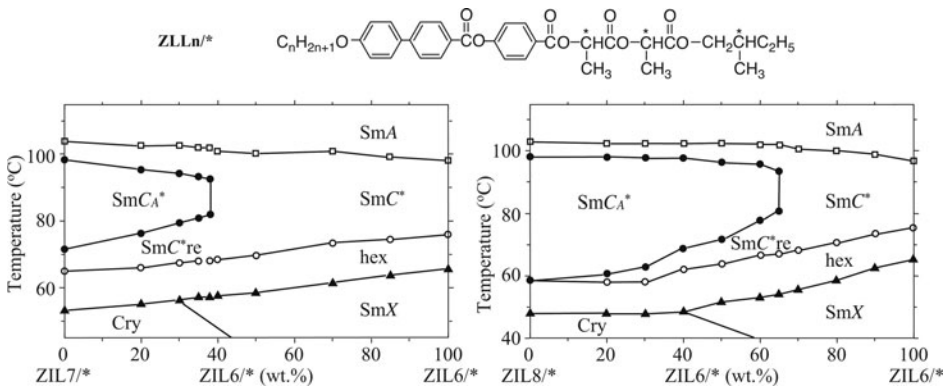

Figure 15. T–r phase diagram of binary mixture systems of ZLL7/*-ZLL6/* and ZLL8/*-ZLL6/*. The re-entrant of ferroelectricity is clearly observed. (From Ref. [54])

The total picture of what molecular interactions are responsible for the emergence of re-entrant SmC^* and/or HxI^* has not become clear yet. There are, however, several illuminating insights into the molecular interactions in the extensive, mainly experimental, studies of the antiferroelectric hexatic phase. It was once considered that the same intermolecular interactions as in SmC_A^* described in Sec. 3.1 are operative and produce the anticlinic structure. Takanishi *et al.* performed detailed studies in MHPOCBC and TFMHPNCBC, and concluded that the corresponding phase is actually HxI_A^*, confirming the tristable switching and the similar X-ray diffraction profiles as observed in HxI^* [55–57]. Neundorf *et al.* [58] and Matkin *et al.* [59] reported that not only antiferroelectric HxI_A^* but also ferroelectric HxI^* also emerges below antiferroelectric SmC_A^*. Neundorf *et al.* obtained the phase diagram of the binary mixture system of (*S*)-MHPOBC and (*R*)-MHOBMB by studying the electric field dependence of conoscopic figures and the temperature dependence of the smectic layer spacing. They showed that HxI_A^* is the high-temperature phase of HxI^* when both emerge, just opposite to the relation between SmC_A^* and SmC^*.

By using sophisticated IR spectroscopic technique, however, Korlacki *et al.* [60] convincingly demonstrated that the antiferroelectric phase that had so far been identified as anticlinic HxI_A^* [55–57] should be better identified as modulated HxB^*, and that the electric-field-induced phase transition from this phase to ferroelectric synclinic HxI^* can be considered as the giant electroclinic effect due to the opening of closed modulation loops. They envisaged the onset of tilting at the SmA-SmC^*/SmC_A^* transition in two different mechanisms: the mutual sliding of molecules and their literal tilting [61, 62]. Actually, Sirota *et al.* [63] pointed out the mutual sliding in 1980's in the generalized phase sequence,

$$\mathrm{Cr}G/\mathrm{Hx}F - \mathrm{Cr}J/\mathrm{HxI} - \mathrm{Cr}B/\mathrm{Hx}B - \mathrm{Sm}C - \mathrm{Sm}A,$$

which is exhibited in many homologous series. In a 2D hexagonal array which represents the projection of molecular centers of mass on a plane normal to the director as illustrated in Fig. 16, Sirota *et al.* made two principal assumptions competing each other: The molecules tend to lie in planes normal to the director, but the most energetically favorable configuration among in-plane nearest neighbors is the one in which the molecules are displaced from each other along the director by a constant percentage of the molecular length; such pairs of molecules were referred to as being connected by a *tilt-bond*. The inherent frustration, caused by the inability of three mutually adjacent molecules to be connected by tilt-bonds, requires that each molecule has on average four tilt-bonds and two *flat-bonds* (contours of constant height) as shown in Fig. 16.

The layer spacing of HxI must be larger than that of HxF, provided that both have the same tilt. HxI must have a larger entropy and appear at higher temperatures of HxF. The entropy can be further increased by allowing the arrows between contours to change the directions and senses. This leads to a structure with reduced net tilt and a greater enthalpy due to the larger layer ripple. Entropy favors a large number of independent arrows, avoiding energy-costly-terminating contours. This can be accomplished by forming closed contour loops of finite size, packed together in some conformation as illustrated in Fig 4 of Ref. [63]. In this way, it is understandable that antiferroelectric HxI_A^* (modulated HxB^*) emerges above ferroelectric HxI^* when both appear, and that the greater enthalpy due to the larger ripple may suppress the emergence of HxI_A^* and hence HxI^* may emerge just below SmC_A^*.

The onset of tilting can be treated in terms of layer undulations and director fluctuations, i.e. the mutual sliding of molecules and their literal tilting, as illustrated in Fig. 1 of Ref. [62]. The literal tilting plays a major role in SmC^*/SmC_A^*, whereas the sliding becomes dominant in HxI^*/HxI_A^* as anticipated in Fig. 16. The sliding and the literal tilting could of course,

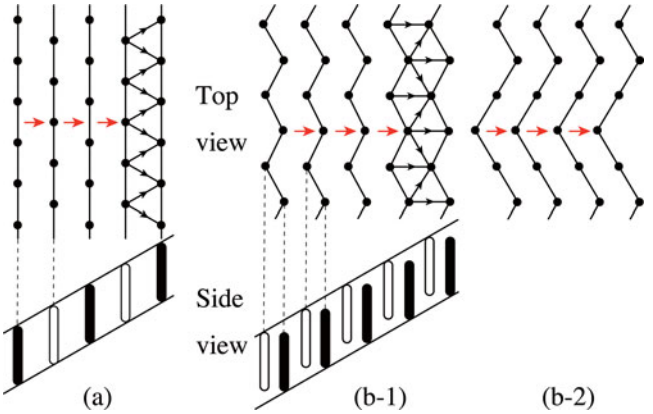

Figure 16. 2D hexagonal arrays that represent the projection of molecular centers of mass on a plane normal to the director in (a) Hx*F*, (b-1) regular Hx*I*, and (b-2) Hx*I* with planar disorder. See text for details. (From Refs. [60] and [63])

in general, occur together; hence we observe, as pretransitional phenomena, some hexatic character in SmC^*/SmC^*_A and undulational fluctuations promoting antiferroelectric HxI^*_A (modulated HxB^*) in ferroelectric HxI^* as well as SmC^*_A. The pretransitional phenomena generally cause an increase in the layer spacing as actually observed by Korlacki *et al.* [60] and by Neundorf *et al.* [58] The presence of two kinds of molecular interactions, one promoting the literal tilting and the other contributing to the sliding, can explain the re-entrant phenomena of ferroelectricity. Thus it is natural to consider the two kinds of frustration of SmC^*_A not only with SmC^* at higher temperatures but also with HxI^* or re-entrant SmC^* at lower temperatures as well as the presence of the critical concentration r^* above which SmC^*_A becomes absolutely unstable. Both the mechanism stabilizes the q_T=1/2 state in an exceptionally wide temperature range, which is responsible for the IR half-pitch reflection pattern.

4. Concluding Remarks

Based on these four-step considerations, we conclude that the IR half-pitch reflection pattern is a manifestation of the TLAF state and can be assigned as the q_T=1/2 state emerging in the narrow range of about 3 wt.% just below the critical concentration r^*, which is stabilized in an exceptionally wide temperature range from about 80°C to room temperature (probably down to −20°C or lower, though not confirmed directly by IR spectroscopy). The TLAF property is endowed by the disclination-assisted thermal linkage between A and F orderings referred to in the 2nd step, which makes the q_T=1/2 state disordered and soft with respect to the tilting directions and senses of the in-layer directors; the electric-field-induced switching is expected to occur layer by layer randomly but not cooperatively. The TLAF state is appropriately designated as SmC^*_D(1/2), where the subscript *D* refers to 'disorder'. The presence of the critical concentration was discussed in connection with the SRILIs stabilizing SmC^*_A in the 1st step as well as the re-entrant phenomena of ferroelectricity in the 4th step. The characteristic feature of q_T=1/2 was explained in connection with the LRILIs in the 3rd step; the surprisingly wide stability range of SmC^*_D(1/2) results from the appearance of HxI^* or re-entrant SmC^* at lower temperatures and its frustration with

SmC_A^* as explained in the 4th step. In this way, there are good reasons for believing the existence of the TLAF SmC_D^*(1/2) phase in the bulk.

As I have pinpointed the narrow concentration region and the unexpectedly wide temperature range of its existence, several experiments are awaiting us to clarify the intriguing aspects of SmC_D^*(1/2) in the bulk. Increasing applied electric field produces nearly the same effects as increasing temperature; both favors the ferroelectric state. Since an applied electric field selectively determines the director tilting sense, however, we should use the number

$$q_E = \frac{|[R] - [L]|}{[R] + [L]} \tag{17}$$

instead of the number q_T given in Eq. (1); here $[R]$ and $[L]$ refer to the numbers of smectic layers with in-layer directors tilted to the Right and to the Left, respectively [64, 65]. In order to prove the TLAF property, we need to show a thresholdless continuous increase of q_E with applied electric field, as we did in Fig. 10 in the case of continuous change of q_T with temperature. It should be noted that applying an electric field also unwinds the macroscopic helical structure of TLAF SmC_D^*(1/2), and that its unwinding process must be quite different from the one in ordinary SmC_A^*(1/2).

The TLAF property in the bulk must be confirmed directly using thick cells aligned either homogeneously ($smectic\ layer\ \perp\ substrate$) or homeotropically ($smectic\ layer\ ||\ substrate$). In fact, Song *et al.* [25] studied the apparent tilt angle as a function of the applied electric field in 9-μm thick homogeneous cells of several MC452 concentration mixtures but missed the $r = 54.99\sim57.50$ wt.% region; they also obtained the apparent polarization vs. applied electric field at $r = 55$ wt.% and confirmed the TLAF property but the cell thickness they used was 2 μm, which is too thin for investigating the bulk property. Among other things, the TLAF property must be nicely confirmed by drawing the *E–T* phase diagrams with Electric-Field-Induced Birefringence (EFIB) contours in 25-μm homeotropic cells of binary mixtures containing $r = 54.99\sim57.50$ wt.% of MC452. Actually, the *E–T* phase diagram Sandhya *et al.* obtained for $r = 57.79$ wt.%, very close to the exact concentrations and shown in Fig. 10(b) of Ref. [12], appears to suggest the TLAF property of SmC_D^*(1/2) although the unwinding process of the macroscopic helical structure seems to occur simultaneously. In the future study, the unwinding process should be observed independently as was done in SmC_A^* by Takanishi *et al.* [66]. Since the TLAF property is endowed by the disclination-assisted thermal linkage between A- and F-orderings, the direct observation of thermal fluctuations by dynamic light scattering or photon correlation spectroscopy [67] must be useful to understand the details of the thermal linkage processes. It is intriguing to know to what extent SmC_D^*(1/2) is made disordered by the disinclination-assisted thermal linkage. I wish I could participate in clarifying these problems in the near future.

Acknowledgments

MGC (Mitsubishi Gas Chemical) is acknowledged for the gift of the precious TLAF liquid crystal compounds. I would like to thank Conference Chairman Jagdish Vij and his Organizing Committee Members for giving me a chance to have this Invited Talk in the 25th ILCC 2014 Dublin; my best thanks are also due to Alexander Emelyanenko for chairing the session.

Appendix: Typographical Error Corrections for Eqs. (68) and (69) of Ref. [43]

Here we keep using the notations in the original paper but not in Sec. 3.3. The linearized simultaneous equations for $(t-1)$ unknown $\Delta\alpha_j$ is given in Eq. (67) of Ref. [43],

$$\sum_{j=0}^{t-2} c_{i,j}\,\Delta\alpha_j = q_i. \tag{A.1}$$

The right hand side q_i is defined as

$$q_i = -2\chi c_{\mathrm{p}} c_{\mathrm{f}} \sum_{n=0}^{i}\sum_{k=i+1}^{t-1} f_{k-n}^{(1)} \cos\varphi_{n,k}^{0}, \tag{A.2}$$

and this should be Eq. (68). The left hand side $c_{i,j}$ is a $(t-1)$ dimensional matrix defined by three equations,
for the lower off-diagonal elements $(i > j)$, j=0, 1, ..., t−3 and i=j+1, j+2, ..., t−2,

$$c_{i,j} = \chi \sum_{n=0}^{j}\sum_{k=i+1}^{t-1} \left\{ c_{\mathrm{p}}^2 f_{k-n} + c_{\mathrm{f}}^2 f_{k-n}^{(2)} \right\} \cos\varphi_{n,k}^{0} + 2B + a\frac{\Delta T}{T^*}\cos\alpha_{t-1}^{0}, \tag{A.3}$$

for the diagonal elements $(j = i)$, $i = j = 0, 1, \ldots, t-2$,

$$c_{i,j} = \chi \sum_{n=0}^{i}\sum_{k=i+1}^{t-1} \left\{ c_{\mathrm{p}}^2 f_{k-n} + c_{\mathrm{f}}^2 f_{k-n}^{(2)} \right\} \cos\varphi_{n,k}^{0} + 4B + a\frac{\Delta T}{T^*}\left(\cos\alpha_{i}^{0} + \cos\alpha_{t-1}^{0}\right), \tag{A.4}$$

and for the upper off-diagonal elements $(i < j)$, $i = 0, 1, \ldots, t-3$ and $j = i+1, i+2, \ldots, t-2$,

$$c_{i,j} = \chi \sum_{n=0}^{i}\sum_{k=j+1}^{t-1} \left\{ c_{\mathrm{p}}^2 f_{k-n} + c_{\mathrm{f}}^2 f_{k-n}^{(2)} \right\} \cos\varphi_{n,k}^{0} + 2B + a\frac{\Delta T}{T^*}\cos\alpha_{t-1}^{0}. \tag{A.5}$$

These three equations should be Eq. (69). Notice that the first term of Eq. (A.4), χ of Eqs. (A.2)–(A.5), and $\Delta T/T^*$ of Eqs. (A.3)–(A.5) are missing in the original paper.

References

[1] Fukuda, A. (1995). *Asia Display 95 Digest*, 61.

[2] Tanaka, C., Fujiyama, T., Maruyama, T., & Nishiyama, S. (1995). *Abstr. Jpn. Liq. Cryst. Conf.*, 250–251.

[3] Inui, S., Iimura, N., Suzuki, T., Iwase, H., Miyachi, K., Takanishi, Y., & Fukuda, A. (1996). *J. Mater. Chem.*, *6*, 671.

[4] Rudquist, P., Lagerwall, J. P. F., Buivydas, M., Gouda, F., Lagerwall, S. T., Clark, N. A., Maclennan, J. E., Shao, R., Coleman, D. A., Bardon, S., Bellini, T., Link, D. R., Natale, G., Glaser, M. A., Walba, D. M., Wand, M. D., Chen, X.-H. (1999a). *J. Mater. Chem.*, 9, 1257.

[5] Rudquist, P., Lagerwall, J. P. F., Buivydas, M., Gouda, F., Lagerwall, S. T., Shao, R. F., Coleman, D., Bardon, S., Link, D. R., Bellini, T., Maclennan, J. E., Walba, D. M., Clark, N. A., Chen, X. H. (1999b). *SID 99 Digest*, 409–411.

[6] Park, B., Seomun, S.-S., Nakata, M., Takahashi, M., Takanishi, Y., Ishikawa, K., & Takezoe, H. (1999a). *Jpn. J. Appl. Phys., Part 1*, *38*, 1474.

[7] Park, B., Nakata, M., Seomun, S.-S., Takanishi, Y., Ishikawa, K., & Takezoe, H. (1999b). *Phys. Rev. E*, 59, R3815.
[8] Seomun, S.-S. (1998). Thesis (Tokyo Institute of Technology).
[9] Matsumoto, T., Fukuda, A., Johno, M., Motoyama, Y., Yui, T., Seomun, S.-S., & Yamashita, M. (1999). *J. Mater. Chem.*, 9, 2051.
[10] Song, J.-K., Chandani, A. D. L., Fukuda, A., Vij, J. K., Kobayashi, I., & Emelyanenko, A. V. (2007a). *Phys. Rev. E*, 76, 011709.
[11] Sandhya, K. L., Chandani-Perera, A. D. L., Fukuda, A., Vij, J. K., & Ishikawa, K. (2010). *Europhys. Lett.*, 90, 56005.
[12] Sandhya, K. L., Chandani, A. D. L., Fukuda, A., Vij, J. K., Emelyanenko, A. V., & Ishikawa, K. (2013a). *Phys. Rev. E*, 87, 012502.
[13] Seomun, S.-S., Gouda, T., Takanishi, Y., Ishikawa, K., Takezoe, H., & Fukuda, A. (1999). *Liq. Cryst.*, 26, 151.
[14] Qian, T., & Taylor, P. L. (1999). *Phys. Rev. E*, 60, 2978.
[15] Parry-Jones, L. A., & Elston, S. J. (2001). *Appl. Phys. Lett.*, 79, 2097.
[16] Hayashi, N., Kato, T., Aoki, T., Ando, T., Fukuda, A., & Seomun, S.-S. (2001). *Phys. Rev. Lett.*, 87, 015701.
[17] Hayashi, N., Kato, T., Aoki, T., Ando, T., Fukuda, A., & Seomun, S. S. (2002). *Phys. Rev. E*, 65, 041714.
[18] Yoshioka, Y., Johno, M., Yui, T., & Matsumoto, T. (2000). *Euro. Pat. Appl.*, EP1039329.
[19] Saishu, T., Takatoh, K., Iida, R., Nagata, H., & Mori, Y. (1996). *SID 96 Digest*, 703–706.
[20] Yoshida, T., Tanaka, T., Ogura, J., Wakai, H., & Aoki, H. (1997). *SID 97 Digest*, 841–844.
[21] Hasegawa, R., Fujiwara, H., Nagata, H., Saishu, T., IIda, R., Hara, Y., Akiyama, M., Okumura, H., & Takatoh, K. (1997). *AM-LCD 97 Digest*, 119–122.
[22] Verhulst, T. (1997). *Jpn. J. Appl. Phys., Part 1*, 36, 720.
[23] Lu, M., Yang, K. H., & Sanford, J. L. (2000). *Ferroelectrics*, 246, 163.
[24] Chan, L. K. M., Bartelous, P., Surguy, P. W. H., Flannigan, N., Swedenkras, G., Waldelof, C., Rampin, M., Vindigni, A., Underwood, I., Vass, D. G., Newsam, M. I., Oton, J. M., Quintana, X. (2000). *Int. Disply Res. Conf. / N. America 00 Digest*, 261–264.
[25] Song, J. K., Fukuda, A., & Vij, J. K. (2008a). *Phys. Rev. E*, 78, 041702.
[26] Chandani, A. D. L. (2007). *Unpublished data in J. K. Vij's Lab. in TCD*.
[27] Panarina, O. (2007). *Unpublished data in J. K. Vij's Lab. in TCD*.
[28] Prost, J., & Bruinsma, R. (1993). *Ferroelectrics*, 148, 25.
[29] Bruinsma, R., & Prost, J. (1994). *J. Phys. (France)*, 4, 1209.
[30] Osipov, M. A., & Fukuda, A. (2000). *Phys. Rev. E*, 62, 3724.
[31] Osipov, M. A., Fukuda, A., & Hakoi, H. (2003). *Mol. Cryst. Liq. Cryst.*, 402, 9.
[32] Fukuda, A., Hakoi, H., Sato, M., & Osipov, M. A. (2003). *Mol. Cryst. Liq. Cryst.*, 398, 169.
[33] Emelyanenko, A. V., Fukuda, A., & Vij, J. K. (2006). *Phys. Rev. E*, 74, 011705.
[34] Emelyanenko, A. V., & Ishikawa, K. (2013). *Soft Matter*, 9, 3497.
[35] Song, J.-K., Fukuda, A., & Vij, J. K. (2008b). *Appl. Phys. Lett.*, 93, 142903.
[36] Li, J.-F., Wang, X.-Y., Kangas, E., Taylor, P. L., Rosenblatt, C., Suzuki, Y. I., & Cladis, P. E. (1995). *Phys. Rev. B*, 52, R13075.
[37] Wang, X. Y., & Taylor, P. L. (1996). *Phys. Rev. Lett.*, 76, 640.
[38] Song, J.-K., Fukuda, A., & Vij, J. K. (2007b). *Phys. Rev. E*, 76, 011708.
[39] Song, J.-K., Fukuda, A., & Vij, J. K. (2008c). *Phys. Rev. Lett.*, 101, 097801.
[40] Li, J., Takezoe, H., & Fukuda, A. (1991). *Jpn. J. Appl. Phys.*, 30, 532.
[41] Gisse, P., Lorman, V. L., Pavel, J., & Nguyen, H. T. (1996). *Ferroelectrics*, 178, 297.
[42] Lagerwall, J. P. F., Giesselmann, F., & Osipov, M. (2006). *Liq. Cryst.*, 33, 625.
[43] Emelyanenko, A. V., & Osipov, M. A. (2003). *Phys. Rev. E*, 68, 051703.
[44] Sandhya, K. L., Vij, J. K., Fukuda, A., & Emelyanenko, A. V. (2009). *Liq. Cryst.*, 36, 1101.
[45] Dolganov, P. V., Zhilin, V. M., Dolganov, V. K., & Kats, E. I. (2011). *Phys. Rev. E*, 83, 061705.
[46] Dolganov, P. V., Zhilin, V. M., Dolganov, V. K., & Kats, E. I. (2012). *Phys. Rev. E*, 86, 020701(R).

[47] Sandhya, K. L., Chandani, A. D. L., Fukuda, A., Kumar, S., & Vij, J. K. (2013b). *Phys. Rev. E*, 87, 062506.
[48] Huang, C. C. (2014). *ILCC 2014 Dublin*, PSO–I2.
[49] Takanishi, Y., & Iida, A. (2014). *ILCC 2014 Dublin*, PSO–I3.
[50] Dolganov, P., Zhilin, V., & Dolganov, V. (2014). *ILCC 2014 Dublin*, PSO–I5.
[51] Emelyanenko, A. V. (2014). *ILCC 2014 Dublin*, PSO–O4–001.
[52] Johnson, P. M., Olson, D. A., Pankratz, S., Nguyen, T., Goodby, J., Hird, M., & Huang, C. C. (2000). *Phys. Rev. Lett.*, 84, 4870.
[53] Cady, A., Pitney, J. A., Pindak, R., Matkin, L. S., Watson, S. J., Gleeson, H. F., Cluzeau, P., Barois, P., Levelut, A.-M., Caliebe, W., et al. (2001). *Phys. Rev. E*, 64, 050702(R).
[54] Novotna, V., Glogarova, M., Hamplova, V., & Kaspar, M. (2001). *J. Chem. Phys.*, 115, 9036.
[55] Takanishi, Y., Takezoe, H., & Fukuda, A. (1993). *Ferroelectrics*, *147*, 135.
[56] Kim, K. H., Takanishi, Y., Ishikawa, K., Takezoe, H., & Fukuda, A. (1994). *Liq. Cryst.*, 16, 185.
[57] Takanishi, Y., Miyachi, K., Yoshida, S., Jin, B., Yin, H., Ishikawa, K., Takezoe, H., & Fukuda, A. (1998). *J. Mater. Chem.*, 8, 1133.
[58] Neundorf, M., Takanishi, Y., Ishikawa, K., Takezoe, H., Fukuda, A., Saito, S., Murashiro, K., Inukai, T., & Demus, D. (1995). *J. Mater. Chem.*, 5, 2221.
[59] Matkin, L. S., Gleeson, H. F., Mach, P., Huang, C. C., Pindak, R., Srajer, G., Pollmann, J., Goodby, J. W., Hird, M., & Seed, A. (2000). *Appl. Phys. Lett.*, 76, 1863.
[60] Korlacki, R., Fukuda, A., & Vij, J. K. (2007). *Europhys. Lett.*, 77, 36004.
[61] Cabib, D., & Benguigui, L. (1977). *J. Phys. (France)*, 38, 419.
[62] Grinstein, G., & Pelcovits, R. A. (1982). *Phys. Rev. A*, 26, 2196.
[63] Sirota, E. B. (1988). *J. Phys. (France)*, 49, 1443.
[64] Fukuda, A., Takanishi, Y., Isozaki, T., Ishikawa, K., & Takezoe, H. (1994). *J. Mater. Chem.*, 4, 997.
[65] Iida, A., Nishiyama, I., & Takanishi, Y. (2014). *Phys. Rev. E*, 89, 032503.
[66] Takanishi, Y., Noma, S., & Yamamoto, J. (2013). *Appl. Phys. Express*, 6, 081701.
[67] Miyachi, K., Kabe, M., Ishikawa, K., Takezoe, H., & Fukuda, A. (1993). *Ferroelectrics*, 147, 147.
[68] TLAF acronym may be used as adjective ‘AntiFerroelectric’ or noun ‘AntiFerroelectricity’ in the following.
[69] They just concluded that the V-shaped switching has its origin in weak inter-layer correlation. Although they referred to the thresholdness behavior in the electric-field-induced change from ferrielectric-like to ferroelectric-like conoscopic figures, this does not indicate any phase transition from ferrielectric to ferroelectric in view of the detailed studies by Song *et al.* [10].
[70] MGC considered that these ferroelectric compounds must be ferrielectric because of their characteristic conoscopic behavior. Song *et al.* clearly showed that these are ferroelectric [10].